

First Measurement of Differential Charged Current Quasielastic-like ν_μ -Argon Scattering Cross Sections with the MicroBooNE Detector

P. Abratenko,³⁵ M. Alrashed,¹⁵ R. An,¹⁴ J. Anthony,⁴ J. Asaadi,³⁴ A. Ashkenazi,¹⁹ S. Balasubramanian,³⁸ B. Baller,¹¹ C. Barnes,²⁰ G. Barr,²⁴ V. Basque,¹⁸ L. Bathe-Peters,¹³ O. Benevides Rodrigues,³¹ S. Berkman,¹¹ A. Bhandari,¹⁸ A. Bhat,³¹ M. Bishai,² A. Blake,¹⁶ T. Bolton,¹⁵ L. Camilleri,⁹ D. Caratelli,¹¹ I. Caro Terrazas,⁸ R. Castillo Fernandez,¹¹ F. Cavanna,¹¹ G. Cerati,¹¹ Y. Chen,¹ E. Church,²⁵ D. Cianci,⁹ E. O. Cohen,³² J. M. Conrad,¹⁹ M. Convery,²⁹ L. Cooper-Troendle,³⁸ J. I. Crespo-Anad3n,⁹ M. Del Tutto,¹¹ D. Devitt,¹⁶ R. Diurba,²¹ L. Domine,²⁹ R. Dorrill,¹⁴ K. Duffy,¹¹ S. Dytman,²⁶ B. Eberly,¹⁰ A. Ereditato,¹ L. Escudero Sanchez,⁴ J. J. Evans,¹⁸ G. A. Fiorentini Aguirre,³⁰ R. S. Fitzpatrick,²⁰ B. T. Fleming,³⁸ N. Foppiani,¹³ D. Franco,³⁸ A. P. Furmanski,²¹ D. Garcia-Gamez,¹² S. Gardiner,¹¹ S. Gollapinni,^{33,17} O. Goodwin,¹⁸ E. Gramellini,¹¹ P. Green,¹⁸ H. Greenlee,¹¹ L. Gu,³⁶ W. Gu,² R. Guenette,¹³ P. Guzowski,¹⁸ E. Hall,¹⁹ P. Hamilton,³¹ O. Hen,¹⁹ G. A. Horton-Smith,¹⁵ A. Hourlier,¹⁹ E.-C. Huang,¹⁷ R. Itay,²⁹ C. James,¹¹ J. Jan de Vries,⁴ X. Ji,² L. Jiang,³⁶ J. H. Jo,³⁸ R. A. Johnson,⁷ Y.-J. Jwa,⁹ N. Kamp,¹⁹ G. Karagiorgi,⁹ W. Ketchum,¹¹ B. Kirby,² M. Kirby,¹¹ T. Kobilarcik,¹¹ I. Kreslo,¹ R. LaZur,⁸ I. Lepetic,¹⁴ K. Li,³⁸ Y. Li,² B. R. Littlejohn,¹⁴ D. Lorca,¹ W. C. Louis,¹⁷ X. Luo,³ A. Marchionni,¹¹ S. Maccocci,¹¹ C. Mariani,³⁶ D. Marsden,¹⁸ J. Marshall,³⁷ J. Martin-Albo,¹³ D. A. Martinez Caicedo,³⁰ K. Mason,³⁵ A. Mastbaum,²⁷ N. McConkey,¹⁸ V. Meddage,¹⁵ T. Mettler,¹ K. Miller,⁶ J. Mills,³⁵ K. Mistry,¹⁸ A. Mogan,³³ T. Mohayai,¹¹ J. Moon,¹⁹ M. Mooney,⁸ A. F. Moor,⁴ C. D. Moore,¹¹ J. Mousseau,²⁰ M. Murphy,³⁶ D. Naples,²⁶ A. Navrer-Agasson,¹⁸ R. K. Neely,¹⁵ P. Nienaber,²⁸ J. Nowak,¹⁶ O. Palamara,¹¹ V. Paolone,²⁶ A. Papadopoulou,¹⁹ V. Papavassiliou,²² S. F. Pate,²² A. Paudel,¹⁵ Z. Pavlovic,¹¹ E. Piasetzky,³² I. D. Ponce-Pinto,⁹ D. Porzio,¹⁸ S. Prince,¹³ X. Qian,² J. L. Raaf,¹¹ V. Radeka,² A. Rafique,¹⁵ M. Reggiani-Guzzo,¹⁸ L. Ren,²² L. Rochester,²⁹ J. Rodriguez Rondon,³⁰ H. E. Rogers,⁵ M. Rosenberg,²⁶ M. Ross-Lonergan,⁹ B. Russell,³⁸ G. Scanavini,³⁸ D. W. Schmitz,⁶ A. Schukraft,¹¹ M. H. Shaevitz,⁹ R. Sharankova,³⁵ J. Sinclair,¹ A. Smith,⁴ E. L. Snider,¹¹ M. Soderberg,³¹ S. S3oldner-Rembold,¹⁸ P. Spentzouris,¹¹ J. Spitz,²⁰ M. Stancari,¹¹ J. St. John,¹¹ T. Strauss,¹¹ K. Sutton,⁹ S. Sword-Fehlberg,²² A. M. Szelc,¹⁸ N. Tagg,²³ W. Tang,³³ K. Terao,²⁹ R. T. Thornton,¹⁷ C. Thorpe,¹⁶ M. Toups,¹¹ Y.-T. Tsai,²⁹ S. Tufanli,³⁸ M. A. Uchida,⁴ T. Usher,²⁹ W. Van De Pontseele,^{24,13} R. G. Van de Water,¹⁷ B. Viren,² M. Weber,¹ H. Wei,² Z. Williams,³⁴ S. Wolbers,¹¹ T. Wongjirad,³⁵ M. Wospakrik,¹¹ W. Wu,¹¹ T. Yang,¹¹ G. Yarbrough,³³ L. E. Yates,¹⁹ G. P. Zeller,¹¹ J. Zennamo,¹¹ and C. Zhang²

(The MicroBooNE Collaboration)*

¹Universit3t Bern, Bern CH-3012, Switzerland

²Brookhaven National Laboratory (BNL), Upton, NY, 11973, USA

³University of California, Santa Barbara, CA, 93106, USA

⁴University of Cambridge, Cambridge CB3 0HE, United Kingdom

⁵St. Catherine University, Saint Paul, MN 55105, USA

⁶University of Chicago, Chicago, IL, 60637, USA

⁷University of Cincinnati, Cincinnati, OH, 45221, USA

⁸Colorado State University, Fort Collins, CO, 80523, USA

⁹Columbia University, New York, NY, 10027, USA

¹⁰Davidson College, Davidson, NC, 28035, USA

¹¹Fermi National Accelerator Laboratory (FNAL), Batavia, IL 60510, USA

¹²Universidad de Granada, E-18071, Granada, Spain

¹³Harvard University, Cambridge, MA 02138, USA

¹⁴Illinois Institute of Technology (IIT), Chicago, IL 60616, USA

¹⁵Kansas State University (KSU), Manhattan, KS, 66506, USA

¹⁶Lancaster University, Lancaster LA1 4YW, United Kingdom

¹⁷Los Alamos National Laboratory (LANL), Los Alamos, NM, 87545, USA

¹⁸The University of Manchester, Manchester M13 9PL, United Kingdom

¹⁹Massachusetts Institute of Technology (MIT), Cambridge, MA, 02139, USA

²⁰University of Michigan, Ann Arbor, MI, 48109, USA

²¹University of Minnesota, Minneapolis, MN, 55455, USA

²²New Mexico State University (NMSU), Las Cruces, NM, 88003, USA

²³Otterbein University, Westerville, OH, 43081, USA

²⁴University of Oxford, Oxford OX1 3RH, United Kingdom

²⁵Pacific Northwest National Laboratory (PNNL), Richland, WA, 99352, USA

²⁶University of Pittsburgh, Pittsburgh, PA, 15260, USA

²⁷*Rutgers University, Piscataway, NJ, 08854, USA*

²⁸*Saint Mary's University of Minnesota, Winona, MN, 55987, USA*

²⁹*SLAC National Accelerator Laboratory, Menlo Park, CA, 94025, USA*

³⁰*South Dakota School of Mines and Technology (SDSMT), Rapid City, SD, 57701, USA*

³¹*Syracuse University, Syracuse, NY, 13244, USA*

³²*Tel Aviv University, Tel Aviv, Israel, 69978*

³³*University of Tennessee, Knoxville, TN, 37996, USA*

³⁴*University of Texas, Arlington, TX, 76019, USA*

³⁵*Tufts University, Medford, MA, 02155, USA*

³⁶*Center for Neutrino Physics, Virginia Tech, Blacksburg, VA, 24061, USA*

³⁷*University of Warwick, Coventry CV4 7AL, United Kingdom*

³⁸*Wright Laboratory, Department of Physics, Yale University, New Haven, CT, 06520, USA*

(Dated: June 3, 2020)

We report on the first measurement of flux-integrated single differential cross sections for charged-current (CC) muon neutrino (ν_μ) scattering on argon with a muon and a proton in the final state, $^{40}\text{Ar}(\nu_\mu, \mu p)X$. The measurement was carried out using the Booster Neutrino Beam at the Fermi National Accelerator Laboratory and the MicroBooNE liquid argon time projection chamber detector with an exposure of 4.59×10^{19} protons on target. Events are selected to enhance the contribution of CC quasielastic (CCQE) interactions, reaching 81.1% of the final event sample. The data are reported in terms of a total cross section as well as single differential cross sections in final state muon and proton kinematics. We measure the integrated CCQE-like cross section of $(4.93 \pm 0.76_{\text{stat}} \pm 1.29_{\text{sys}}) \times 10^{-38} \text{cm}^2$, in good agreement with theoretical calculations. The single differential cross sections are also in overall good agreement with theoretical predictions, except at very forward muon scattering angles that correspond to low momentum-transfer events.

Measurements of neutrino oscillation serve as a valuable tool for extracting neutrino mixing angles, mass-squared differences, and the CP violating phase, as well as for searching for new physics beyond the standard model in the electroweak sector [1, 2].

Neutrinos oscillate as a function of their propagation distance divided by their energy. In accelerator-based oscillation experiments, the neutrino propagation distance is well defined. However, as these experiments do not use mono-energetic neutrino beams [3–5], the accuracy to which they can extract neutrino oscillation parameters depends on their ability to determine the individual energy of the detected neutrinos. This requires detailed understanding of the fundamental interactions of neutrinos with atomic nuclei that comprise neutrino detectors.

Understanding the interaction of neutrinos with argon nuclei is of particular importance as a growing number of neutrino oscillation experiments employ liquid argon time projector chamber (LArTPC) neutrino detectors. These include the Deep Underground Neutrino Experiment (DUNE) [6–9], which aims to measure the neutrino CP-violating phase and mass hierarchy, and the Short Baseline Neutrino (SBN) program [10], that is searching for physics beyond the Pontecorvo–Maki–Nakagawa–Sakata (PMNS) matrix model of neutrino mixing.

Experimentally, the energy of interacting neutrinos is determined from the measured momenta of particles that are emitted following the neutrino interaction in the detector. Many accelerator-based oscillation studies focus on measurements of charged-current (CC) neutrino-nucleon quasielastic (QE) scattering interactions [11–20], where the neutrino removes a single intact nucleon from

the nucleus without producing any additional particles. This choice is guided by the fact that CCQE reactions can be reasonably well approximated as two-body interactions, and their experimental signature of a correlated muon-proton pair is relatively straightforward to measure. Therefore, precise measurements of CCQE processes are expected to allow precise reconstruction of neutrino energies with discovery-level accuracy [21].

A working definition for identifying CCQE interactions in experimental measurements requires the identification of a neutrino interaction vertex with an outgoing lepton, exactly one outgoing proton, and no additional particles; We refer to these herein as CCQE-like events. This definition can include contributions from non-CCQE interactions that lead to the production of additional particles that are absent from the final state due to nuclear effects such as pion absorption or have momenta that are below the experimental detection threshold.

Existing data on neutrino CCQE-like interactions come from experiments using various energies and target nuclei [22]. These primarily include measurements of CCQE-like muon neutrino (ν_μ) cross sections for interactions where a muon and no pions were detected, with [17–20] and without [11–16] requiring the additional detection of a proton in the final state. While most relevant for LArTPC based oscillation experiments, no measurements of CCQE-like cross sections on ^{40}Ar with the detection of a proton in the final state exist.

This letter presents the first measurement of exclusive CCQE-like neutrino-argon interaction cross-sections, measured using the MicroBooNE liquid argon time projection chamber (LArTPC). Our data serve as the first

study of exclusive CCQE-like differential cross sections on ^{40}Ar as well as a benchmark for theoretical models of ν_{μ} - ^{40}Ar interactions, which are key for performing a precise extraction of oscillation parameters by future LArTPC oscillation experiments.

We focus on a specific subset of CCQE-like interactions, denoted here as CC1p0 π , where the contribution of CCQE interactions is enhanced [23]. These include charged-current ν_{μ} - ^{40}Ar scattering events with a detected muon and exactly one proton, with momenta greater than 100 MeV/ c and 300 MeV/ c , respectively. The measured muon-proton pairs are required to be coplanar with small missing transverse momentum and minimal residual activity near the interaction vertex that is not associated with the measured muon or proton. For these CC1p0 π events we measure the flux-integrated ν_{μ} - ^{40}Ar total and differential cross sections in muon and proton final state kinematics: $d\sigma/dp_{\mu}$, $d\sigma/d\cos\theta_{\mu}$, $d\sigma/dp_p$, and $d\sigma/d\cos\theta_p$. Here, p_{μ} , θ_{μ} , p_p , and θ_p are the momenta and the in-plane scattering angles of the muon and proton, respectively. In addition, we extract the cross section as a function of the calorimetric measured energy and the reconstructed momentum transfer.

The measurement uses data from the MicroBooNE LArTPC detector [24], which is the first of a series of LArTPCs to be used for precision oscillation measurements [6–10, 25]. The MicroBooNE detector has an active mass of 85 tons and is located along the Booster Neutrino Beam (BNB) at Fermilab, 463 m downstream from the target. The BNB energy spectrum extends to 2 GeV and peaks around 0.7 GeV [3].

A neutrino is detected by its interaction with an argon nucleus in the LArTPC. The secondary charged particles produced in the interaction travel through the liquid argon, leaving a trail of ionization electrons that drift horizontally and transverse to the neutrino beam direction in an electric field of 273 V/cm, to a system of three anode wire planes located 2.5 m from the cathode plane. The Pandora tracking package [26] is used to form individual particle tracks from the measured ionization signals. Particle momenta are determined from the measured track length for protons and multiple Coulomb scattering pattern for muons [27].

Thirty-two photomultiplier tubes (PMTs) are placed outside the TPC, facing the active volume, to collect argon scintillation light. Events are retained (triggered) if the PMT signals are in time-coincidence with the beam arrival time. A sample within an off-beam gate is also collected. At nominal running conditions, a neutrino interaction is expected in approximately 500 BNB beam spills. The PMT trigger condition increases the fraction of recorded spills with a neutrino interaction to $\approx 10\%$. Application of additional software selection further rejects background events, mostly from cosmic muons, to provide an analysis sample that contains a neutrino in-

teraction in $\approx 15\%$ of the selected spills [28, 29]. The analysis presented here is performed on data collected from the BNB beam, with an exposure of 4.59×10^{19} protons on target (POT).

The selected CC1p0 π event definition includes events with any number of protons with momenta below 300 MeV/ c , neutrons at any momenta, and charged pions with momentum lower than 70 MeV/ c . The minimal proton momentum requirement of 300 MeV/ c is guided by its stopping range in LAr and corresponds to five wire pitches in the TPC, to ensure an efficient particle identification.

To avoid contributions from cosmic tracks, our CC1p0 π selection considers only pairs of tracks with a fully-contained proton candidate and a fully or partially contained muon candidate in the fiducial volume of the MicroBooNE detector. The fiducial volume is defined by $3 < x < 253$ cm, $-110 < y < 110$ cm, and $5 < z < 1031$ cm. The x axis points along the negative drift direction with 0 cm placed at the anode plane, y points vertically upward with 0 cm at the center of the detector, and z points along the direction of the beam, with 0 cm at the upstream edge of the detector. Tracks are fully contained if both the start point and end point are within this volume and partially contained if only the start point is within this volume.

The event selection and background rejection used for this analysis are described in detail in Ref. [23], only in this work the proton momentum detection threshold was raised from 200 MeV/ c to 300 MeV/ c . Muon-proton pair candidates are identified by requiring two tracks with a common vertex and an energy deposition profile, dE/dx , that is consistent with that expected for a muon and a proton in our LArTPC. We further require that the muon track is longer than the proton track, that the PMT response is higher than that typically measured for cosmic tracks and that the PMTs with the highest signal are located close to the muon-proton pair interaction vertex. We suppress broken cosmic tracks (i.e., a single cosmic ray that interacts and is reconstructed as two tracks) by requiring that the opening angle $\Delta\theta_{\mu,p}$ between the measured muon-proton pair is greater than 35° or smaller than 145° (i.e., $|\Delta\theta_{\mu,p} - 90^\circ| < 55^\circ$). See online supplementary materials for details.

We limit our analysis to a phase space region where the detector response to our signal is well understood and its effective detection efficiency is higher than 2.5%. This corresponds to $0.1 < p_{\mu} < 1.5$ GeV/ c , $0.3 < p_p < 1.0$ GeV/ c , $-0.65 < \cos\theta_{\mu} < 0.95$, and $\cos\theta_p > 0.15$. Additional kinematical selections are used to enhance the contribution of CCQE interactions in our CC1p0 π sample. These include requiring that the measured muon-proton pairs be coplanar ($|\Delta\phi_{\mu,p} - 180^\circ| < 35^\circ$), have small missing momentum transverse relative to the beam direction ($p_T = |\vec{p}_T^{\mu} + \vec{p}_T^p| < 350$ MeV/ c), and have a small energy deposition around the interaction vertex that is not

associated with the muon or proton tracks.

We estimate that our efficiency for selecting CC1p0 π CCQE-like events is $\approx 20\%$, with a purity of $\approx 84\%$ [23] and a CCQE contribution of $\approx 81\%$. After the application of the event selection requirement, we retain 410 CC1p0 π candidate events.

We report single differential cross sections in measured proton and muon kinematics. First, three-dimensional differential cross sections are measured and then integrated to form the total and the single-differential cross sections. We follow this procedure because of the statistical limitations of the data set. As additional data become available, it will allow extracting multi-dimensional differential cross sections.

The three-fold differential cross sections are given by:

$$\left(\frac{d^3\sigma}{dp_\mu d\cos\theta_\mu d\phi_\mu} \right)_n = \frac{N_n^{\text{on}} - N_n^{\text{off}} - B_n}{\epsilon_n^\mu \cdot \Phi_\nu \cdot N_{\text{target}} \cdot \Delta_n^\mu}, \quad (1)$$

and

$$\left(\frac{d^3\sigma}{dp_p d\cos\theta_p d\phi_p} \right)_n = \frac{N_n^{\text{on}} - N_n^{\text{off}} - B_n}{\epsilon_n^p \cdot \Phi_\nu \cdot N_{\text{target}} \cdot \Delta_n^p}, \quad (2)$$

where, in each bin n , N_n^{on} is the number of measured events when the beam is on, N_n^{off} is number of measured events when the beam is off (i.e., cosmic-induced background events), B is the beam-related background (estimated from Monte Carlo (MC) simulation), N_{target} is the number of scattering nuclei, Φ_ν is the integrated incoming neutrino flux, Δ_n^μ and Δ_n^p are the differential bin widths. ϵ_n^μ (ϵ_n^p) is the simulated effective muon (proton) detection efficiency, defined as the ratio of the number of reconstructed CC1p0 π events to the number of true generated CC1p0 π events in bin n . This procedure accounts for bin migration effects such that cross-sections are obtained as a function of real (as oppose to experimentally reconstructed) kinematical variables. See online supplementary materials for details.

The presentation of data here as two three-fold rather than a single six-fold differential cross section is dictated by the limited data and simulation statistics. It is justified since the proton and muon efficiencies are largely

TABLE I: Integrated cross sections for data and various GENIE models. Results are listed for the full measured phase space and for a limited one of $\cos(\theta_\mu) < 0.8$.

		Integrated Cross Section [10^{-38}cm^2]	
		$-0.65 < \cos(\theta_\mu) < 0.95$	$-0.65 < \cos(\theta_\mu) < 0.8$
Data CC1p0 π		4.93 ± 1.55	4.05 ± 1.40
GENIE	Nominal	6.18	4.04
	hA2015	6.37	4.14
	Alternative	6.69	4.64
	v3.0.6	5.45	3.66

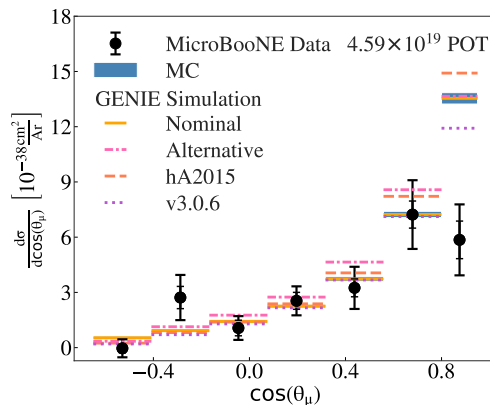


FIG. 1: The flux integrated single differential CC1p0 π cross sections as a function of the cosine of the measured muon scattering angle. Inner and outer error bars show the statistical and total (statistical and systematic) uncertainty at the 1 σ , or 68%, confidence level. Colored lines show the results of theoretical absolute cross section calculations using the GENIE event generator (without passing through a detector simulation) [30, 31]. The blue band shows the extracted cross section obtained from analyzing MC events propagated through our full detector simulation. The width of the band denotes the simulation statistical uncertainty.

independent in the region of interest, and this effect is accounted for in the systematic uncertainties.

The extracted cross sections are expected to be independent of the azimuthal angle ϕ . However, the simple model used to simulate the effect of induced charge on neighboring TPC wires leads to a low reconstruction efficiency of tracks perpendicular to the wire planes ($\phi \approx 0$ and $\phi \approx \pm\pi$) that created an artificial ϕ dependence to the cross section. We correct for this effect using an iterative procedure. We first reweight events with a muon track falling in the $\phi \approx 0$ bin and $|\sin\theta| > 0.3$ to the weighted average of the cross sections in all other bins of ϕ_μ where $|\sin\theta| > 0.3$. Due to the coplanarity requirement, this reweighting affects the distribution of $\phi_p \approx \pm\pi$. We repeat the process starting from a proton track with $\phi_p \approx 0$ until the cross section change is less than 0.01%, typically after 5 iterations.

TABLE II: χ^2 values for the agreement between various GENIE models and the measured differential cross sections. Results are listed for the full measured phase space and for a limited one of $\cos(\theta_\mu) < 0.8$.

GENIE	Differential Cross Section $\chi^2/\text{d.o.f}$	
	$-0.65 < \cos(\theta_\mu) < 0.95$	$-0.65 < \cos(\theta_\mu) < 0.8$
Nominal	63.2/28	30.1/27
hA2015	56.5/28	25.4/27
Alternative	51.2/28	33.7/27
v3.0.6	34.6/28	21.4/27

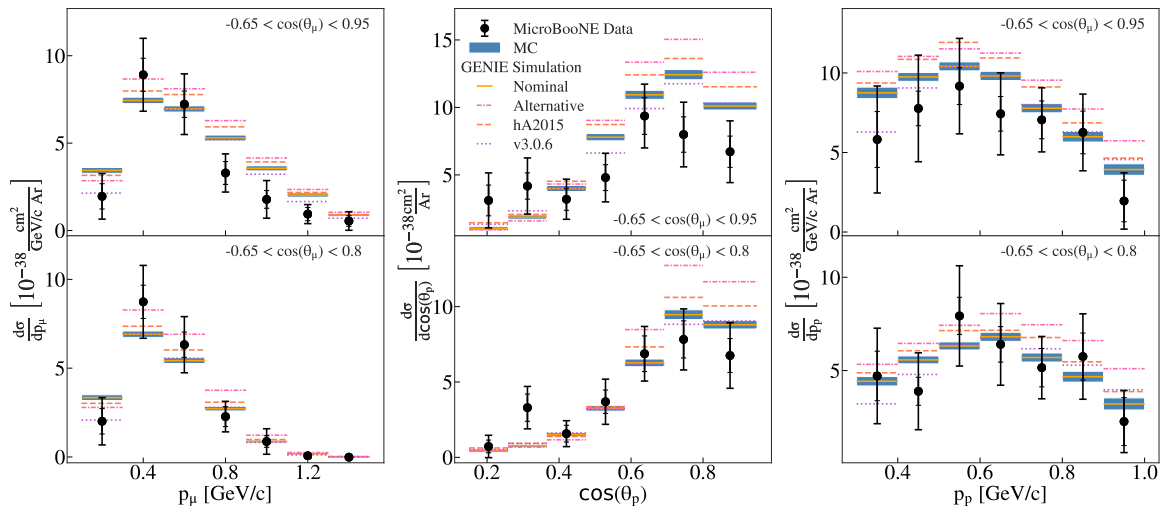


FIG. 2: As Fig. 1, but for the differential cross sections as a function of measured muon momentum (left) and measured proton scattering angle (middle) and momentum (right). Cross sections are shown for the full measured phase-space (top) and for events with $\cos(\theta_\mu) < 0.8$ (bottom).

The integrated measured CC1p0 π cross section is summarized in Table I. The statistical uncertainty of our measurement is 15.9%. The systematic uncertainty sums to 26.2% and includes contributions from the neutrino flux prediction and POT estimation (18.7%), detector response modeling (18.4%), imperfect proton and muon efficiency decoupling (5.7%), and neutrino interaction cross section modeling (7.1%).

The neutrino flux is predicted using the flux simulation of the MiniBooNE Collaboration that used the same beam line [13]. We account for the small distance between MiniBooNE and MicroBooNE. Neutrino cross section modeling uncertainties were estimated using the GENIE framework of event reweighting [30, 31] with its standard reweighting parameters. For both cross section and flux systematics, we use a multisim technique [32], which consists of generating many MC replicas, each one called a “universe”, where model parameters are varied within their uncertainties. Each universe represents a different reweighting. The simultaneous reweighting of all model parameters allows the correct treatment of their correlations.

A different model is followed for detector model systematic uncertainties, that are dominated by individual detector parameters. Unisim samples [32] are generated, where one detector parameter is varied each time by 1σ . We then examine the impact of each parameter variation on the extracted cross sections, by obtaining the differences with respect to the central value on a bin-by-bin basis. One exception is the systematic uncertainty due to induced charge effects mentioned above that include the data-driven correction and are thus estimated separately. See online supplementary materials for details. We then define the total detector 1σ systematic uncertainty by

summing in quadrature the effect of each individual variation.

The MC simulation used to estimate the backgrounds and effective efficiency contains real cosmic data overlaid onto a neutrino interaction simulation that uses GENIE [30, 31] to simulate both the signal events and the beam backgrounds. See Ref. [23] for details. For the simulated portion, the particle propagation is based on Geant4 [33], while the simulation of the MicroBooNE detector is performed in the LArSoft framework [34, 35]. The beam-related background subtracted from the CC1p0 π events is simulated.

Fig. 1 shows the flux integrated single differential CC1p0 π cross section as a function of the cosine of the measured muon scattering angle. The data are compared to several theoretical calculations and to our GENIE-based MC prediction. The latter is the result of analyzing a sample of MC events produced using our “nominal” GENIE model and propagated through the full detector simulation in the same way as data. The theoretical predictions are calculated using the GENIE event generator [30, 31], with no detector simulation, for four different models:

- **Nominal:** GENIE v2.12.2 with the Bodek-Ritchie Fermi Gas model, the Llewellyn-Smith CCQE scattering prescription [36], and the empirical meson exchange current (MEC) model [37], a Rein-Sehgal resonance (RES) and coherent scattering (COH) model [38], and a data driven final state interaction (FSI) model denoted as “hA” [39].
- **hA2015:** GENIE v2.12.2 with the Bodek-Ritchie Fermi Gas model, a more recent “hA2015” FSI model with Oset medium correction for pions [30, 31].

- **Alternative:** GENIE v2.12.10 with the Local Fermi Gas model [40], the Nieves CCQE scattering prescription [41], the Nieves MEC model [42], the KLN-BS RES [43–46] and BS COH [47] scattering models, and the hA2015 FSI model.
- **v3.0.6:** Using the same comprehensive model configuration as the Alternative model, only with hA2018 FSI model [48].

The agreement between the “nominal” GENIE calculation and the MC prediction constitutes a closure test for our analysis.

As can be seen in Fig. 1, all GENIE predictions are in overall good agreement with our data, except for the highest $\cos\theta_\mu$ bin, where the measured cross section is significantly lower than the theoretical predictions.

The observed discrepancy between data and theory for high $\cos\theta_\mu$ cannot be explained by the systematic uncertainties and is therefore indicative of an issue with the theoretical models. Specifically, high $\cos\theta_\mu$ correspond to low momentum transfer events which were previously observed to not be well reproduced by theory in inclusive reactions [15, 16] and is now also seen in exclusive reactions.

As the differential cross sections in proton kinematics and muon momentum include contributions from all muon scattering angles, their agreement with the theoretical calculation is affected by this disagreement. Fig. 2 shows this comparison between the relevant cross sections in the full available phase-space (top) and in the case where events with $\cos\theta_\mu > 0.8$ are excluded (bottom). Removing this part of the phase-space significantly improves the agreement between data and theory. Table II lists the χ^2 for the agreement of the different GENIE models with the data for differential cross sections for the full available phase-space and for $\cos\theta_\mu < 0.8$. Systematic uncertainties and correlations were accounted for using covariance matrices. The χ^2 values reported in the table are the simple sum of those χ^2 values obtained for each distribution separately. As can be seen, the $\chi^2/\text{d.o.f.}$ in the $\cos\theta_\mu < 0.8$ sample is reduced by a factor of ~ 2 as compared to the full available phase-space sample. See online supplementary material for details.

Lastly, Fig. 3 shows the flux-integrated single differential cross sections as a function of calorimetric measured energy and reconstructed momentum transfer, with and without events with $\cos\theta_\mu > 0.8$. The former is defined as $E_\nu^{\text{cal}} = E_\mu + T_p + BE$, and the latter as $Q_{CCQE}^2 = (\vec{p}_\nu - \vec{p}_\mu)^2 - (E_\nu^{\text{cal}} - E_\mu)^2$, where E_μ is the muon energy, T_p is the proton kinetic energy, $BE = 40$ MeV is the effective nucleon binding energy for ^{40}Ar , and $\vec{p}_\nu = (0, 0, E_\nu^{\text{cal}})$ is the reconstructed interacting neutrino momentum. E_ν^{cal} is often used as a proxy for the reconstructed neutrino energy.

Overall, good agreement is observed between data and calculations for these complex variables, even for the full

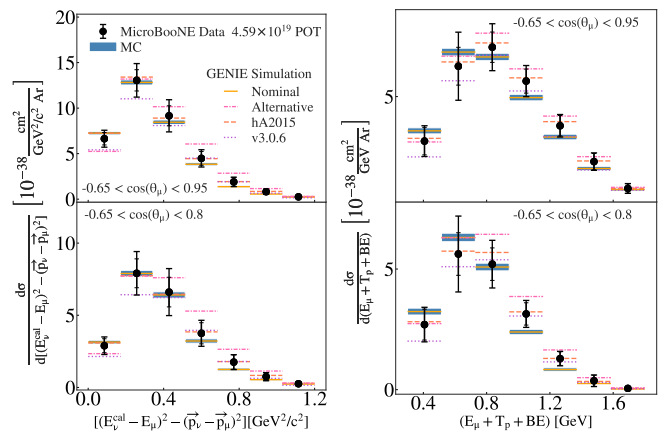


FIG. 3: The flux integrated single differential CC1p0 π cross sections as a function of $Q_{CCQE}^2 = (E_\nu^{\text{cal}} - E_\mu)^2 - (\vec{p}_\nu - \vec{p}_\mu)^2$ and $E_\nu^{\text{cal}} = E_\mu + T_p + BE$, where $BE = 40$ MeV and $\vec{p}_\nu = (0, 0, E_\nu^{\text{cal}})$. Inner and outer error bars show the statistical and total (statistical and systematic) uncertainty at the 1σ , or 68%, confidence level. Colored lines show the results of theoretical absolute cross section calculations using the GENIE event generator (without passing through a detector simulation). The blue band shows the extracted cross section obtained from analyzing MC events passed through our full detector simulation.

event sample without the $\cos\theta_\mu < 0.8$ requirement.

In summary, we report the first measurement of ν_μ CCQE-like differential cross sections on ^{40}Ar for event topologies with a single muon and a single proton detected in the final state. The data are in good agreement with GENIE predictions, except at small muon scattering angles that correspond to low momentum-transfer reactions. This measurement confirms and constrains calculations essential for the extraction of oscillation parameters and highlights kinematic regimes where improvement of theoretical models is required. The benchmarking of exclusive CC1p0 π cross sections on ^{40}Ar presented here suggests that measurements of CC1p0 π interactions are a suitable choice for use in precision neutrino oscillation analyses, especially after theoretical models are reconciled with the small scattering angle data.

This document was prepared by the MicroBooNE collaboration using the resources of the Fermi National Accelerator Laboratory (Fermilab), a U.S. Department of Energy, Office of Science, HEP User Facility. Fermilab is managed by Fermi Research Alliance, LLC (FRA), acting under Contract No. DE-AC02-07CH11359. MicroBooNE is supported by the following: the U.S. Department of Energy, Office of Science, Offices of High Energy Physics and Nuclear Physics; the U.S. National Science Foundation; the Swiss National Science Foundation; the Science and Technology Facilities Council (STFC), part of the United Kingdom Research and Innovation; and The Royal Society (United Kingdom). Additional support for the laser calibration system and cosmic ray

tagger was provided by the Albert Einstein Center for Fundamental Physics, Bern, Switzerland. The work presented in this manuscript was supported in part by the Azrieli Foundation, Israel Science Foundation, Visiting Scholars Award Program of the Universities Research Association, and the Zuckerman STEM Leadership Program.

* microboone.info@fnal.gov

- [1] M. Tanabashi *et al.* (Particle Data Group), “Review of particle physics,” *Phys. Rev. D* **98**, 030001 (2018).
- [2] K. Abe *et al.* (T2K), “Constraint on the matter-antimatter symmetry-violating phase in neutrino oscillations,” *Nature* **580**, 339 (2020).
- [3] A.A. Aguilar-Arevalo *et al.* (MiniBooNE), “The Neutrino Flux prediction at MiniBooNE,” *Phys. Rev. D* **79**, 072002 (2009), [arXiv:0806.1449 \[hep-ex\]](https://arxiv.org/abs/0806.1449).
- [4] L. Aliaga *et al.* (MINERvA Collaboration), “Neutrino Flux Predictions for the NuMI Beam,” [10.1103/PhysRevD.94.092005](https://arxiv.org/abs/10.1103/PhysRevD.94.092005).
- [5] K. Abe *et al.* (T2K Collaboration), “T2K neutrino flux prediction,” [10.1103/PhysRevD.87.012001](https://arxiv.org/abs/10.1103/PhysRevD.87.012001).
- [6] Babak Abi *et al.* (DUNE), “Deep Underground Neutrino Experiment (DUNE), Far Detector Technical Design Report, Volume I Introduction to DUNE,” (2020), [arXiv:2002.02967 \[physics.ins-det\]](https://arxiv.org/abs/2002.02967).
- [7] Babak Abi *et al.* (DUNE), “Deep Underground Neutrino Experiment (DUNE), Far Detector Technical Design Report, Volume II DUNE Physics,” (2020), [arXiv:2002.03005 \[hep-ex\]](https://arxiv.org/abs/2002.03005).
- [8] Babak Abi *et al.* (DUNE), “Deep Underground Neutrino Experiment (DUNE), Far Detector Technical Design Report, Volume III DUNE Far Detector Technical Coordination,” (2020), [arXiv:2002.03008 \[physics.ins-det\]](https://arxiv.org/abs/2002.03008).
- [9] Babak Abi *et al.* (DUNE), “Deep Underground Neutrino Experiment (DUNE), Far Detector Technical Design Report, Volume IV Far Detector Single-phase Technology,” (2020), [arXiv:2002.03010 \[physics.ins-det\]](https://arxiv.org/abs/2002.03010).
- [10] M. Antonello *et al.* (MicroBooNE, LAr1-ND, ICARUS-WA104 Collaborations), “A Proposal for a Three Detector Short-Baseline Neutrino Oscillation Program in the Fermilab Booster Neutrino Beam,” (2015), [arXiv:1503.01520 \[physics.ins-det\]](https://arxiv.org/abs/1503.01520).
- [11] C. Anderson *et al.* (ArgoNeuT Collaboration), “First Measurements of Inclusive Muon Neutrino Charged Current Differential Cross Sections on Argon,” *Phys. Rev. Lett.* **108**, 161802 (2012).
- [12] Y. Nakajima *et al.* (SciBooNE Collaboration), “Measurement of Inclusive Charged Current Interactions on Carbon in a Few-GeV Neutrino Beam,” *Phys. Rev. D* **83**, 012005 (2011).
- [13] A.A. Aguilar-Arevalo *et al.* (MiniBooNE Collaboration), “First measurement of the muon antineutrino double-differential charged-current quasielastic cross section,” *Phys. Rev. D* **88**, 032001 (2013).
- [14] K. Abe *et al.* (T2K Collaboration), “Measurement of the ν_μ charged-current quasielastic cross section on carbon with the ND280 detector at T2K,” *Phys. Rev. D* **92**, 112003 (2015).
- [15] M.F. Carneiro *et al.* (MINERvA Collaboration), “High-Statistics Measurement of Neutrino Quasielastic-Like Scattering at $E_\nu \sim 6$ GeV on a Hydrocarbon Target,” *Phys. Rev. Lett.* **124**, 121801 (2020).
- [16] P. Abratenko *et al.* (MicroBooNE Collaboration), “First Measurement of Inclusive Muon Neutrino Charged Current Differential Cross Sections on Argon at $E_\nu \sim 0.8$ GeV with the MicroBooNE Detector,” *Phys. Rev. Lett.* **123**, 131801 (2019).
- [17] G.A. Fiorentini *et al.* (MINERvA Collaboration), “Measurement of Muon Neutrino Quasielastic Scattering on a Hydrocarbon Target at $E_\nu \sim 3.5$ GeV,” *Phys. Rev. Lett.* **111**, 022502 (2013).
- [18] M. Betancourt *et al.* (MINERvA Collaboration), “Direct Measurement of Nuclear Dependence of Charged Current Quasielasticlike Neutrino Interactions Using MINERvA,” *Phys. Rev. Lett.* **119**, 082001 (2017).
- [19] T. Walton *et al.* (MINERvA Collaboration), “Measurement of muon plus proton final states in ν_μ interactions on hydrocarbon at $\langle E_\nu \rangle = 4.2$ GeV,” *Phys. Rev. D* **91**, 071301 (2015).
- [20] K. Abe *et al.* (T2K Collaboration), “Characterization of nuclear effects in muon-neutrino scattering on hydrocarbon with a measurement of final-state kinematics and correlations in charged-current pionless interactions at T2K,” *Phys. Rev. D* **98**, 032003 (2018).
- [21] U. Mosel *et al.*, “Energy reconstruction in the Long-Baseline Neutrino Experiment,” *Phys. Rev. Lett.* **112**, 151802 (2014).
- [22] J.A. Formaggio and G.P. Zeller, “From eV to EeV: Neutrino Cross Sections Across Energy Scales,” *Rev. Mod. Phys.* **84**, 1307–1341 (2012).
- [23] C. Adams *et al.* (MicroBooNE Collaboration), “Rejecting cosmic background for exclusive charged current quasi elastic neutrino interaction studies with Liquid Argon TPCs; a case study with the MicroBooNE detector,” *Eur. Phys. J. C* **79**, 673 (2019).
- [24] R. Acciarri *et al.* (MicroBooNE Collaboration), “Design and Construction of the MicroBooNE Detector,” *J. Instrum.* **12**, P02017 (2017).
- [25] F. Tortorici, V. Bellini, and C.M. Sutura (ICARUS), “Upgrade of the ICARUS T600 Time Projection Chamber,” *J. Phys. Conf. Ser.* **1056**, 012057 (2018).
- [26] R. Acciarri *et al.* (MicroBooNE Collaboration), “The Pandora multi-algorithm approach to automated pattern recognition of cosmic-ray muon and neutrino events in the MicroBooNE detector,” *Eur. Phys. J. C* **78**, 82 (2018).
- [27] P. Abratenko *et al.* (MicroBooNE Collaboration), “Determination of muon momentum in the MicroBooNE LArTPC using an improved model of multiple Coulomb scattering,” *J. Instrum.* **12**, P10010 (2017).
- [28] D. Kaleko *et al.*, “PMT Triggering and Readout for the MicroBooNE Experiment,” *J. Instrum.* **8**, C09009 (2013).
- [29] C. Adams *et al.* (MicroBooNE Collaboration), “Ionization electron signal processing in single phase LArTPCs. Part II. Data/simulation comparison and performance in MicroBooNE,” *J. Instrum.* **13**, P07007 (2018).
- [30] C. Andreopoulos *et al.*, *Nucl. Instrum. Meth. A*, 87–104.
- [31] C. Andreopoulos *et al.*, “The GENIE Neutrino Monte Carlo Generator: Physics and User Manual,” (2015), [arXiv:1510.05494 \[hep-ph\]](https://arxiv.org/abs/1510.05494).
- [32] B.P. Roe, “Statistical errors in Monte Carlo estimates of systematic errors,” *Nucl. Instrum. Meth. A* **570**, 159–164

- (2007).
- [33] S. Agostinelli *et al.* (GEANT4 Collaboration), Nucl. Instrum. Meth. **A 506** (2003).
- [34] R. Pordes and E. Snider, “The Liquid Argon Software Toolkit (LArSoft): Goals, Status and Plan,” *PoS ICHEP2016*, 182 (2016).
- [35] E. Snider and G. Petrillo, “LArSoft: Toolkit for Simulation, Reconstruction and Analysis of Liquid Argon TPC Neutrino Detectors,” *J. Phys. Conf. Ser.* **898**, 042057 (2017).
- [36] C.H. Llewellyn Smith, “Neutrino Reactions at Accelerator Energies,” *Phys. Rept.* **3**, 261–379 (1972).
- [37] T. Katori, “Meson Exchange Current (MEC) Models in Neutrino Interaction Generators,” *AIP Conf. Proc.* **1663**, 030001 (2015).
- [38] D. Rein and L. Sehgal, “Neutrino Excitation of Baryon Resonances and Single Pion Production,” *Annals Phys.* **133**, 79–153 (1981).
- [39] S.G. Mashnik *et al.*, “CEM03 and LAQGSM03: New modeling tools for nuclear applications,” *J. Phys. Conf. Ser.* **41**, 340–351 (2006).
- [40] R.C. Carrasco and E. Oset, “Interaction of Real Photons With Nuclei From 100-MeV to 500-MeV,” *Nucl. Phys. A* **536**, 445–508 (1992).
- [41] J. Nieves, F. Sanchez, I. Ruiz Simo, and M.J. Vicente Vacas, “Neutrino Energy Reconstruction and the Shape of the CCQE-like Total Cross Section,” *Phys. Rev. D* **85**, 113008 (2012).
- [42] J. Schwehr, D. Cherdack, and R. Gran, “GENIE implementation of IFIC Valencia model for QE-like 2p2h neutrino-nucleus cross section,” (2016), [arXiv:1601.02038 \[hep-ph\]](https://arxiv.org/abs/1601.02038).
- [43] J. A. Nowak (MiniBooNE Collaboration), “Four Momentum Transfer Discrepancy in the Charged Current π^+ Production in the MiniBooNE: Data vs. Theory,” *AIP Conf. Proc.* **1189**, 243–248 (2009).
- [44] K. Kuzmin *et al.*, “Lepton polarization in neutrino nucleon interactions,” *Phys. Part. Nucl.* **35**, S133–S138 (2004).
- [45] Ch. Berger and L.M. Sehgal, “Lepton mass effects in single pion production by neutrinos,” *Phys. Rev. D* **76**, 113004 (2007).
- [46] K. M. Graczyk and J. T. Sobczyk, “Form Factors in the Quark Resonance Model,” *Phys. Rev. D* **77**, 053001 (2008), [Erratum: *Phys.Rev.D* 79, 079903 (2009)].
- [47] C. Berger and L. Sehgal, “PCAC and coherent pion production by low energy neutrinos,” *Phys. Rev. D* **79**, 053003 (2009).
- [48] D. Ashery, I. Navon, G. Azuelos, H.K. Walter, H.J. Pfeiffer, and F.W. Schlepütz, “True Absorption and Scattering of Pions on Nuclei,” *Phys. Rev. C* **23**, 2173–2185 (1981).